Supporting Information for

Using green emitting pH-responsive nanogels to report environmental changes within hydrogels: A nanoprobe for versatile sensing

Mingning Zhu[a,*], Dongdong Lu[a], Shanglin Wu[a], Qing Lian[a], Wenkai Wang[a], L. Andrew Lyon[b], Weiguang Wang[c], Paulo Bártolo[c] and Brian R. Saunders[a,*]

[a]*School of Materials, University of Manchester, MSS Tower, Manchester, M13 9PL, U.K.*

[b]*Schmid College of Science and Technology, Chapman University, Orange, CA, 92866, USA.*

[c]*Manchester Institute of Biotechnology, School of Mechanical, Aerospace and Civil Engineering, University of Manchester, Manchester M13 9PL, UK*

Corresponding authors:

Mingning Zhu: mingning.zhu@manchester.ac.uk

Brian R. Saunders: brian.saunders@manchester.ac.uk

Table of Contents

EXPERIMENTAL DETAILS

Absolute photoluminescence quantum yields

For absolute photoluminescence quantum yields (PLQY) measurements, the PLQY values were acquired using an integrating sphere incorporated into the FLS980 spectrofluorometer over a range of emission wavelengths and measured in a quartz sample holder. The PLQY was calculated with FLS 980 software using the equation[1]:

$$\Phi_{overall} = \frac{S(Em)}{S(Abs)} = \frac{\int \frac{\lambda}{hc}[I_{sample(em)}(\lambda) - I_{reference(em)}(\lambda)]d\lambda}{\int \frac{\lambda}{hc}[I_{reference(ex)}(\lambda) - I_{sample(ex)}(\lambda)]d\lambda} \tag{1}$$

where $S(Abs)$ is the number of photons absorbed by the sample and $S(Em)$ is the number of photons emitted from the sample, λ is the wavelength, h is Planck's constant, c is the velocity of light, $I_{sample(ex)}$ and $I_{reference(ex)}$ are the integrated intensities of the excitation beam with and without the sample, and $I_{sample(em)}$ and $I_{reference(em)}$ are the PL intensities with and without the sample, respectively.

PL intensity dependence on pH-triggered swelling and collapse measurements

Dispersions: The PL and DLS measurements were conducted using NG$_{AM/BDP}$ dispersions (0.01 wt.%) diluted in 0.10 M PDP buffer. The PDP buffer solutions used were phosphate based[2]. For the measurement of the reversible performance of pH response, the NG$_{AM/BDP}$ dispersion (0.020 wt.%) in PDP buffer (pH 6.0) was placed in dialysis tubing and this was placed in a much greater volume of buffer solution, which was periodically switched from pH 6.0 to 8.0. A period of 24 h was allowed for the internal pH to equilibrate at the new pH value.

Gels: DX NG-*MAA*(NG$_{AM/BDP)}$ and Gelatin(NG$_{AM/BDP}$) gels were prepared sandwiched within an o-ring (outer diameter = 13 mm, inner diameter = 9 mm and thickness = 1 mm) using glass slides. After preparation they were transferred to containers with fresh buffer (0.10 M) of various pH

values. Each sample weight and PL spectra were obtained with an equilibration time of 24 h then returned to a fresh solution.

PL reporting of divalent cationic triggered gel deswelling

Dispersions: The DLS and PL measurements were conducted using $NG_{AM/BDP}$ dispersions (0.010 wt.%) diluted in various Mg^{2+} concentration solution using 0.020 M increments in aqueous $MgSO_4$ solutions at pH 7.4 via PDP buffer solution. For the other cations (Ca^{2+}, Mg^{2+}, Zn^{2+}, K^+, Ba^{2+}, Sr^{2+}), $NG_{AM/BDP}$ dispersions (0.010 wt.%) were diluted in the respective metal salt solutions (30 mM) at pH 8.6; whilst for Zn^{2+} pH 7.4 was used with the aid of adjustment with NaOH.

Gels: For DX NG-*MAA*($NG_{AM/BDP}$), the gels were transferred to containers with solutions containing variable ions (Ca^{2+}, Mg^{2+}, K^+) concentrations at pH 7.4. The measurement in pure water was used as a control. Each sample weight and PL spectra were obtained with an equilibration time of 24 h then returned to a fresh solution.

PL reporting of temperature-triggered hydrogel swelling changes

All temperature detection experiments were carried out in stoppered quartz dishes (Interior 10 x 10 x 48 mm) and 9 °C increments were used for the gels. The equilibrium temperature time was 30 min. For covalent DX NG-*OEG* ($NG_{AM/BDP}$) hydrogel experiment, the entire quartz contained DX NG-*OEG*($NG_{AM/BDP}$) was transferred to pH 6.0 buffer solution for 3 days. For the measurement of the reversible performance of temperature response, all test samples were subject to temperature changes from 4.0 to 40 °C in quartz. They were equilibrated for 30 min between measurements. The swelling of DX NG-*OEG* ($NG_{AM/BDP}$) hydrogel was equilibrated at each temperature for 24 h. For these measurements the *Q* values were determined from the gel dimensions.

PL reporting of Gelatin degradation

To measure ratio of the degradation in vitro, disk-shaped Gelatin($NG_{AM/BDP}$) hydrogels (92.5 mg)

were immersed in a 7.0 ml glass vial with PDP buffer solution (2.0 mL, pH 7.4) which were kept at 32 °C. After soaking for an interval of time, all the mixtures were drawn from buffer solution and transferred to quartz cuvette to measure UV and PL then placed back in the incubator. The degradation ratio (%) was calculated using the absorbance at 507 nm.

Tensile strain-dependent PL study

PAAm-Clay(NG$_{AM/BDP}$) hydrogel was sandwiched in a cuboid mold (length = 65 mm, width = 20 mm, height = 1.5 mm). Samples were taken out of the mold and cut into pieces (20 x 6.8 x 1.5 mm) and placed on transparent quartz slides for FLS 980 detector remotely. Small clips secured the ends of the PAAm-Clay(NG$_{AM/BDP}$) hydrogels and were used to change the strain.

Non-radiative energy transfer (NRET) analysis

The spectra used for the following were measured at pH 8.0. The PL spectra of NG$_{AM}$ was measured using an excitation wavelength of 254 nm (Fig. S2A). The UV-visible absorption spectrum of NG$_{BDP}$ was also measured (see Fig. S2B). The standard curves for Lambert-Beer law for BDP are shown in the Fig S1(B). The NG$_{AM}$ emission spectrum for acceptor nanogels (NG$_{BDP}$) at pH 8.0 values was used to calculate the spectral overlap integral[3]:

$$J(\lambda) = \int I(\lambda)\varepsilon_A(\lambda)\lambda^4 d\lambda \qquad \text{(S1)}$$

where $I(\lambda)$ is the integrated intensity of the emission spectrum of the NG$_{AM}$ donor in the range 370-650 nm wavelength, ε_A is the molar extinction coefficient of the NG$_{BDP}$ acceptor at pH 8.0, and λ is the wavelength (nm). For NG$_{AM/BDP}$ nanoprobe, $J(\lambda)$ was calculated to be 4.58 x 10^{-14} M^{-1} cm^{-3}. The latter was used to calculate the Förster distance, R_0, i.e., the distance between the donor and acceptor at which the NRET efficiency is 50%. The R_0 value was calculated using[4]

$$R_0^6 = \left(8.785 \times 10^{-5}\right)\kappa^2 \varphi J \eta^{-4} \qquad \text{(S2)}$$

where κ^2 is the dipole orientation factor. A random orientation of the donor and acceptor moieties

was assumed so that the value used was $2/3$[5]. φ is the absolute PLQY of the donor NG$_{AM}$. The PLQY was 18.4% which was determined using integrating sphere over a range of emission wavelengths (370 to 650 nm). The refractive index, η, of the medium (PMMA) used was 1.49[5].

Imaging of cell uptake

Human adipose-derived stem cells ranging from passage 7 to 9 were cultured with Gibco™ MesenPRO RS™ Basal Medium (Invitrogen) supplemented with MesenPRO RS™ Growth Supplement in T75 tissue culture flasks. The cells were washed three times using 0.05% trypsin solution (Invitrogen) trypsinized until 80% confluence and re-suspended on 60 mm culture plates. Subsequently, the cells in each well were suspended in 1.0 mL of PBS and centrifuged at 1200 rpm for 2.5 min. After removing the supernatants, the cells were re-suspended in 0.3 mL of PBS. Quantity data for cells per well were collected, and analyses were performed using a Nexcelom Bioscience cellometer auto 1000. 150 µL of medium containing around 5.0×10^4 cells were then seeded on each 24-well plate containing 310 µL medium at pH 7.4 or 6.0, and 40 µL the NG$_{AM/BDP}$ nanoprobe dispersions were respectively added to each plate and carefully mixed. The final concentration of nanoprobe was 10 µg/mL and incubation was for 4 h at 5% CO_2, 95% humidity and 37 °C environment. After incubation, the plates were washed thoroughly with sterile PBS and fixed with 10% (w/v) neutral buffered formalin for 30 min at room temperature. Subsequently, samples were rinsed three times with PBS for the removal of formalin, permeabilized with 0.5 mL 0.1 % Triton-X100 (Sigma-Aldrich, Dorset, UK) in PBS at room temperature for 10 minutes, rinsed three times for the removal of Triton-X100. Afterwards, 500 µL of 8% FBS solution was added into each sample and incubated for 60 min at room temperature to block non-specific binding. The cells were stained with Alexa Fluor 594 phalloidin at the manufacturer recommended concentration for cell actin protein 45 min at room temperature and were washed rapidly three times with PBS. Finally, samples were left in the staining solution for 10 min prior to removal, rinsed twice thoroughly with PBS, and images for the nanoprobe uptake experiments were obtained with a Leica

CLSM (λ_{ex} = 405 nm). In the study, images of red-emitted cellular organelles (Alexa Fluor 594) and green or blue-emitted nanoprobe particles were acquired in optical windows between 570 - 800 nm, 500 - 570 nm and 406 - 500 nm, respectively.

SCHEMES
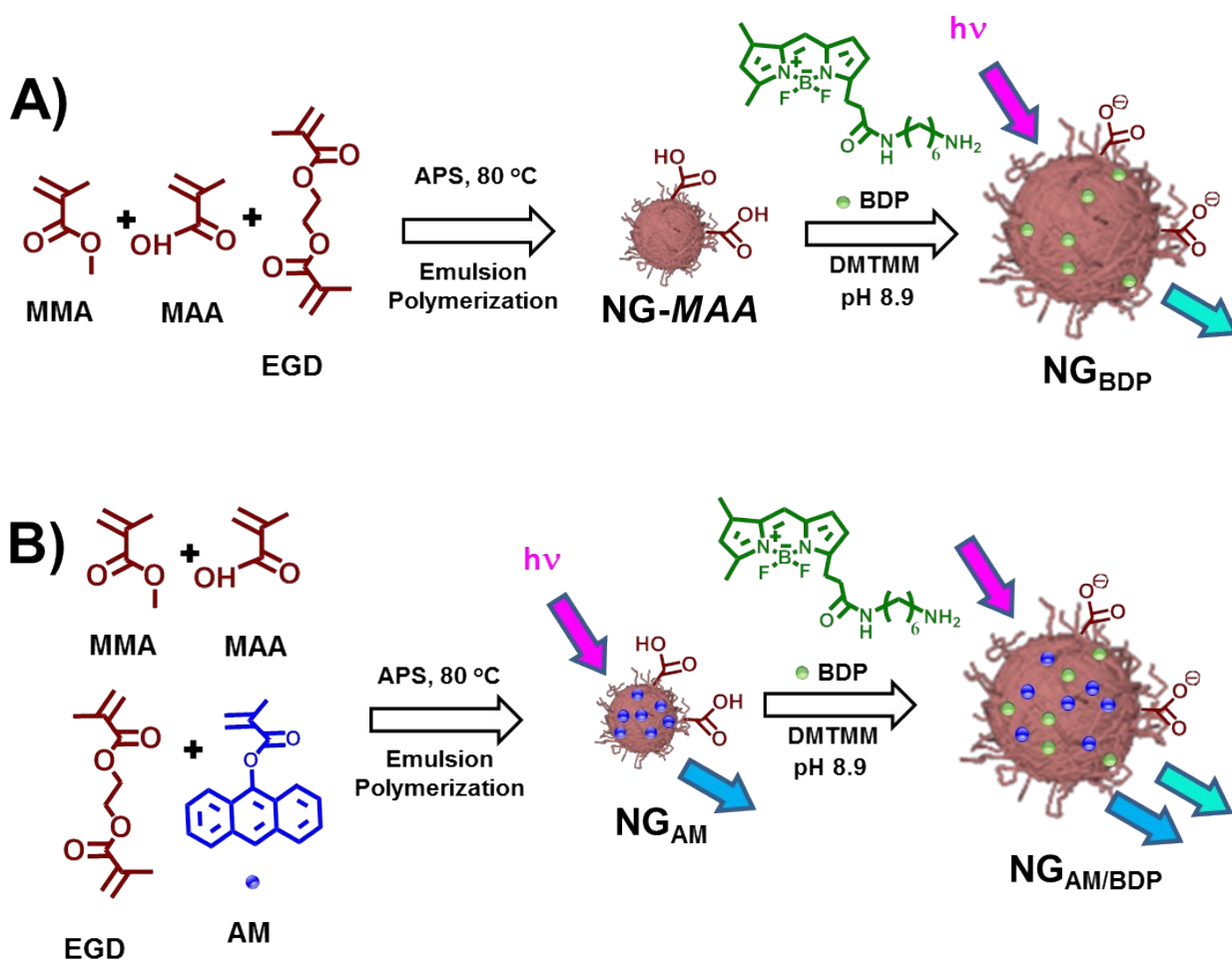
Scheme S1. Depiction of the synthesis of the **(A)** NG_{BDP} and **(B)** NG_{AM} as well as $NG_{AM/BDP}$ probe particles. BDP FL amine (BDP) and (9-anthryl)methacrylate (AM) were the acceptor and donor, respectively.
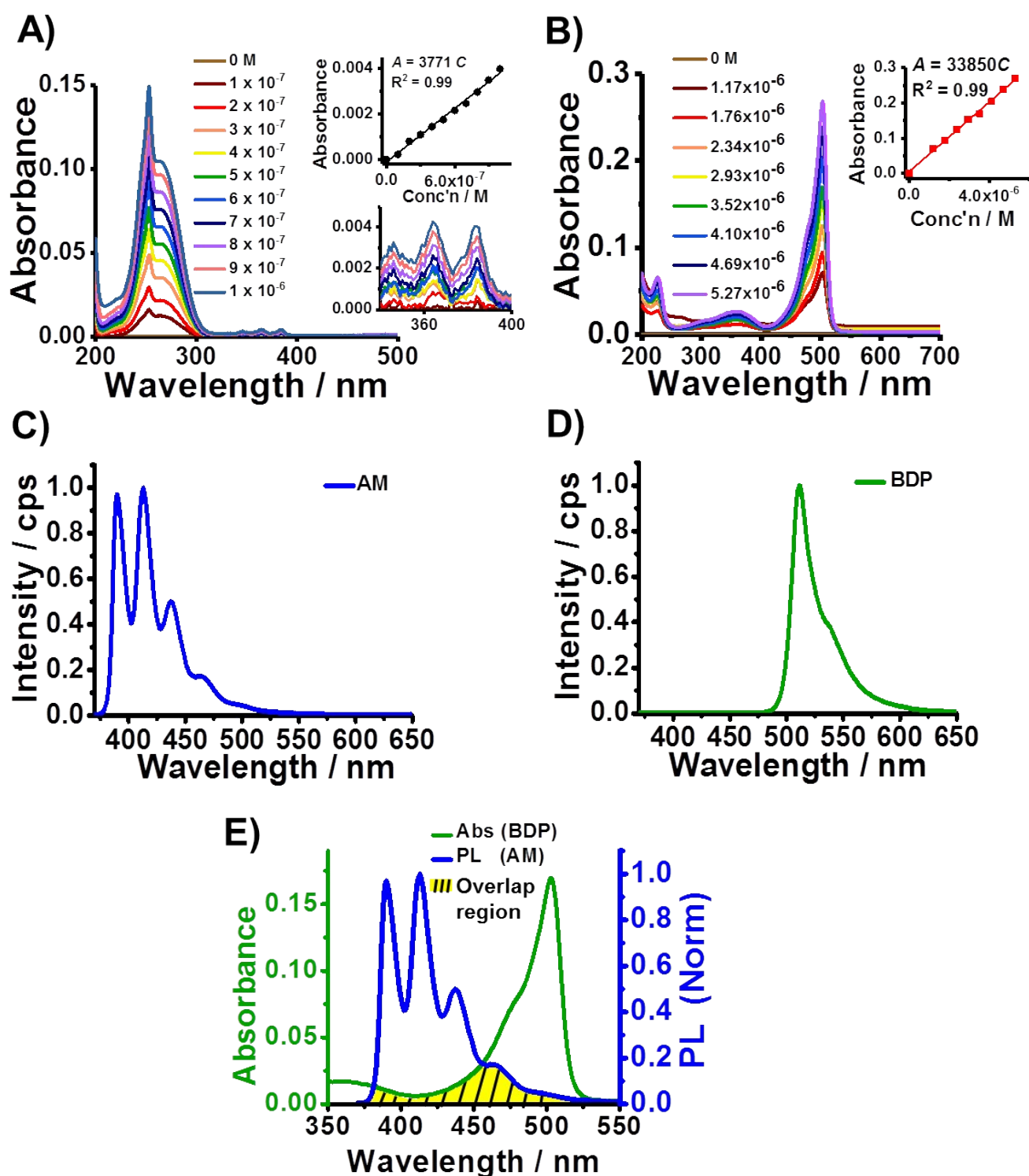
FIGURES

Figure S1. Characterisation of AM and BDP. UV-visible spectra for **(A)** AM and **(B)** BDP at various concentrations in water. Normalised PL spectra for **(C)** AM and **(D)** BDP in water. **(E)** Overlap region between the emission from the AM donor and the absorption of the BDP acceptor.
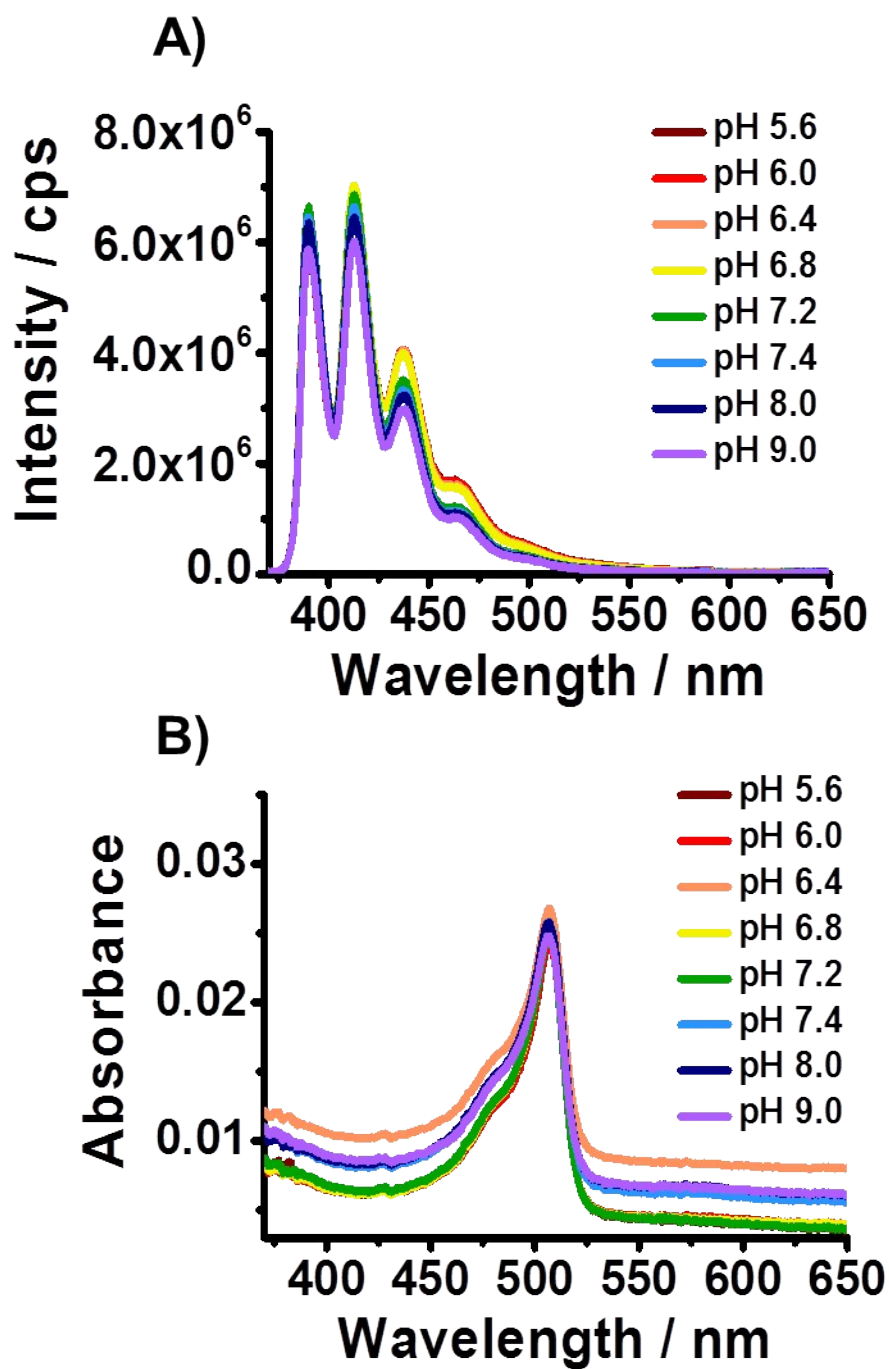
Figure S2. Characterisation of NG_{AM} and NG_{BDP}. **(A)** PL spectra ($\lambda_{ex} = 254$ nm) for NG_{AM} and **(B)** UV-visible spectra for NG_{BDP} obtained at various pH values.

A)

B)

C)
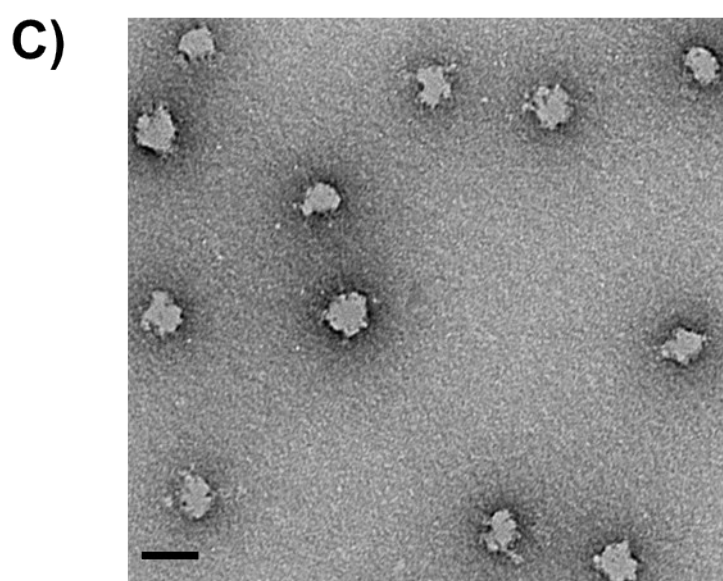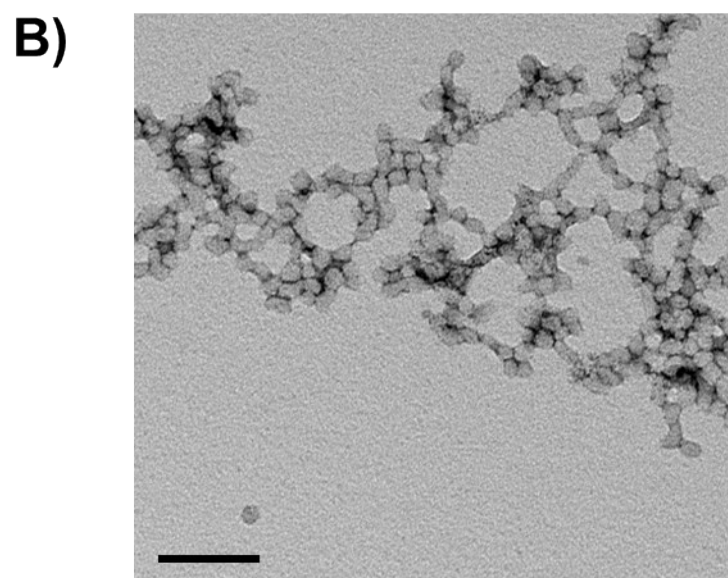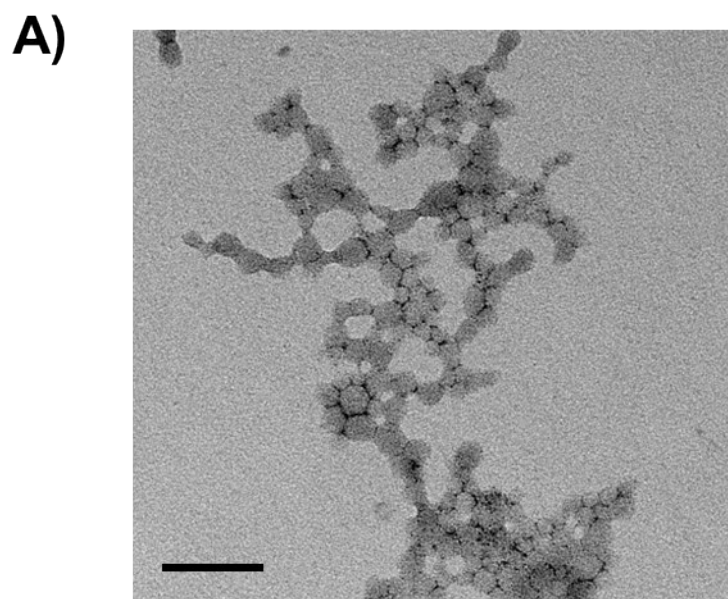
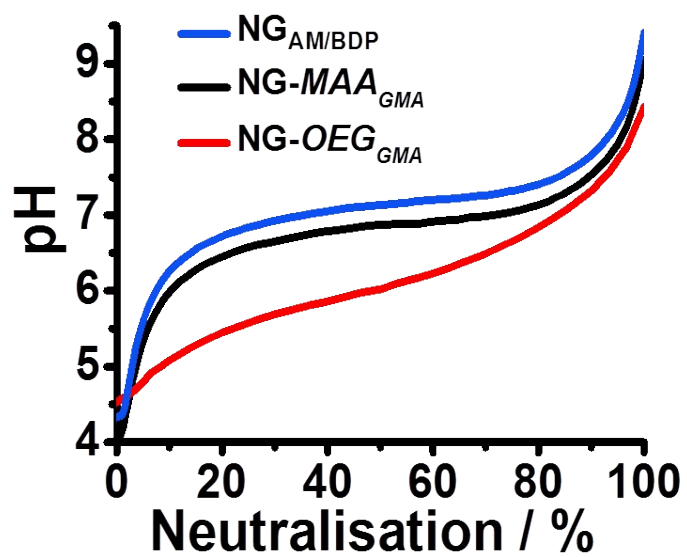**Figure S3.** TEM for (A) NG$_{\text{AM/BDP}}$, (B) NG-*MAA*$_{\text{GMA}}$ and (C) NG-*OEG*$_{\text{GMA}}$. Scale bars: 100 nm.

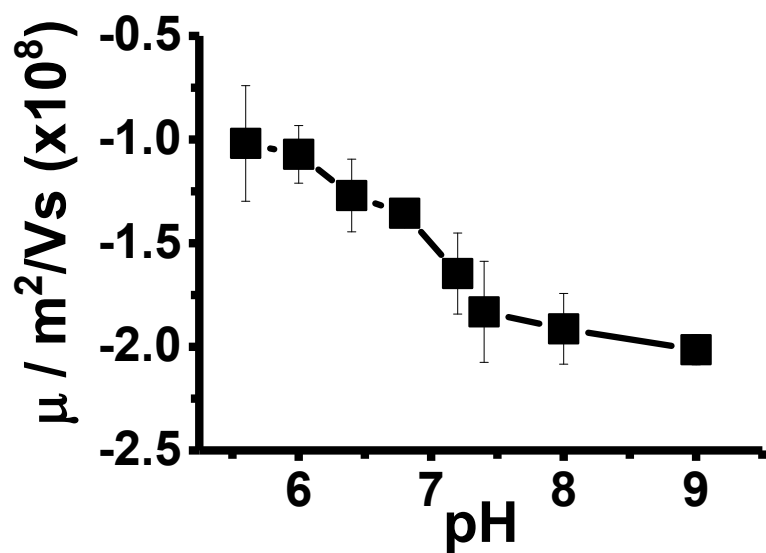**Figure S4.** Titration data for various NGs. The apparent pK_a was obtained from the pH at 50% neutralisation.

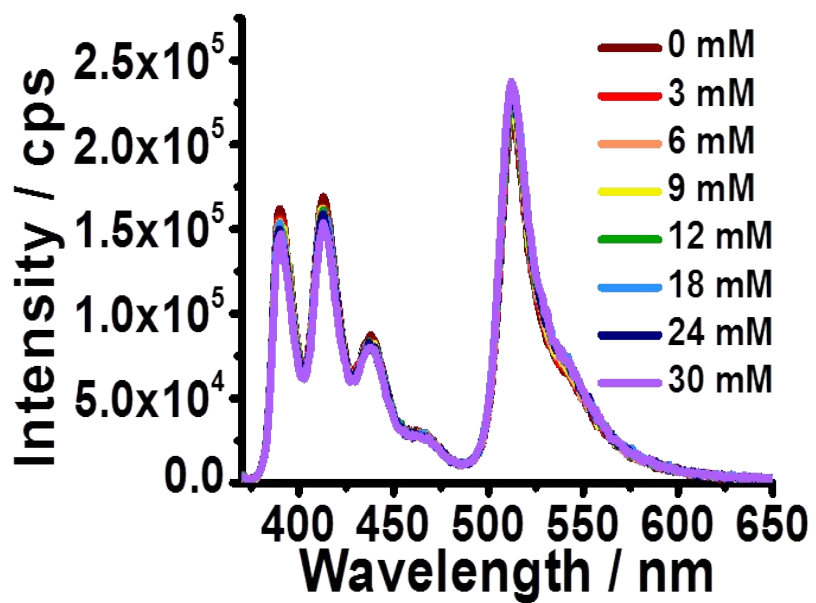**Figure S5.** Electrophoretic mobility as a function of pH for $NG_{AM/BDP}$.

Figure S6. PL spectra (λ_{ex} = 365 nm) for NG$_{AM/BDP}$ obtained at various Mg^{2+} concentrations (pH 7.4).
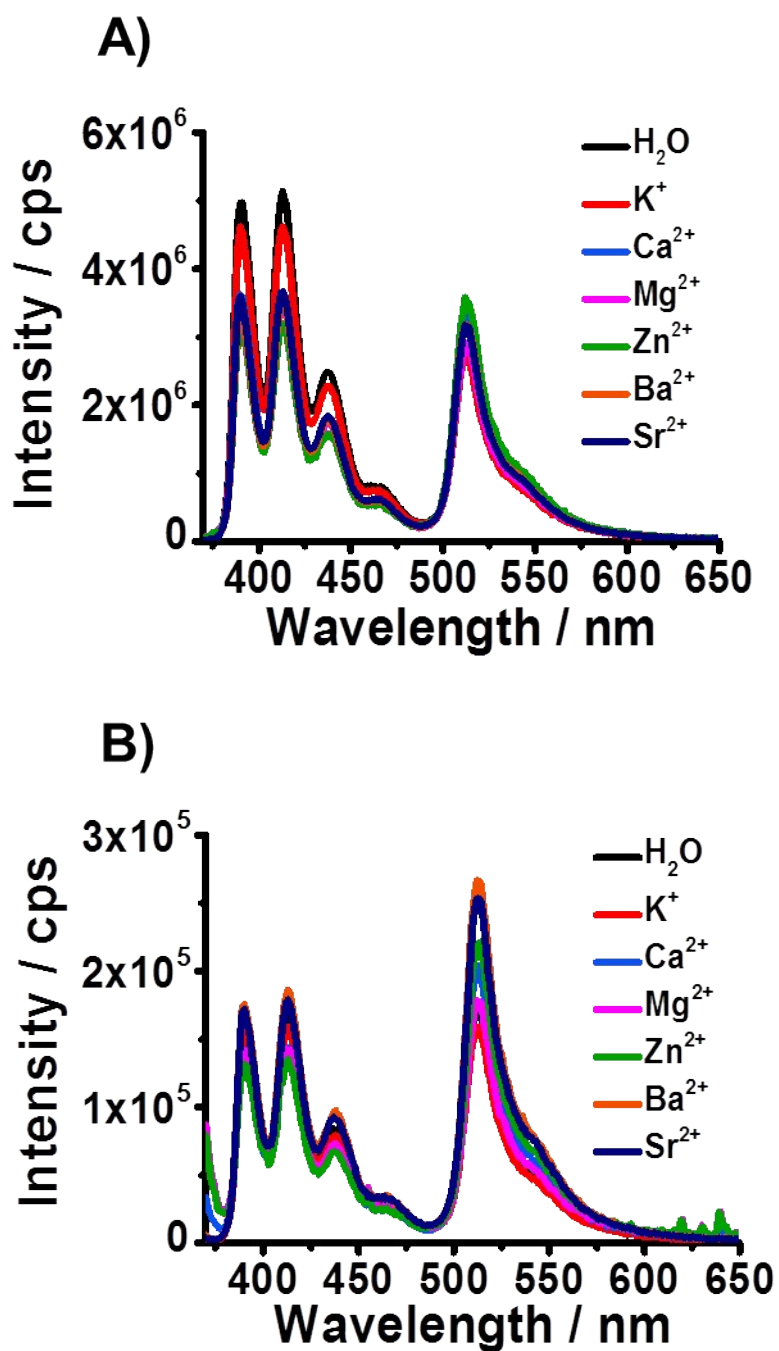
Figure S7. PL spectra for NG$_{AM/BDP}$ under 254 nm **(A)** and 365 nm **(B)** excitation measured using 30 mM of various ions. The pH used was 8.6 except for Zn^{2+}, where the pH was 7.4.
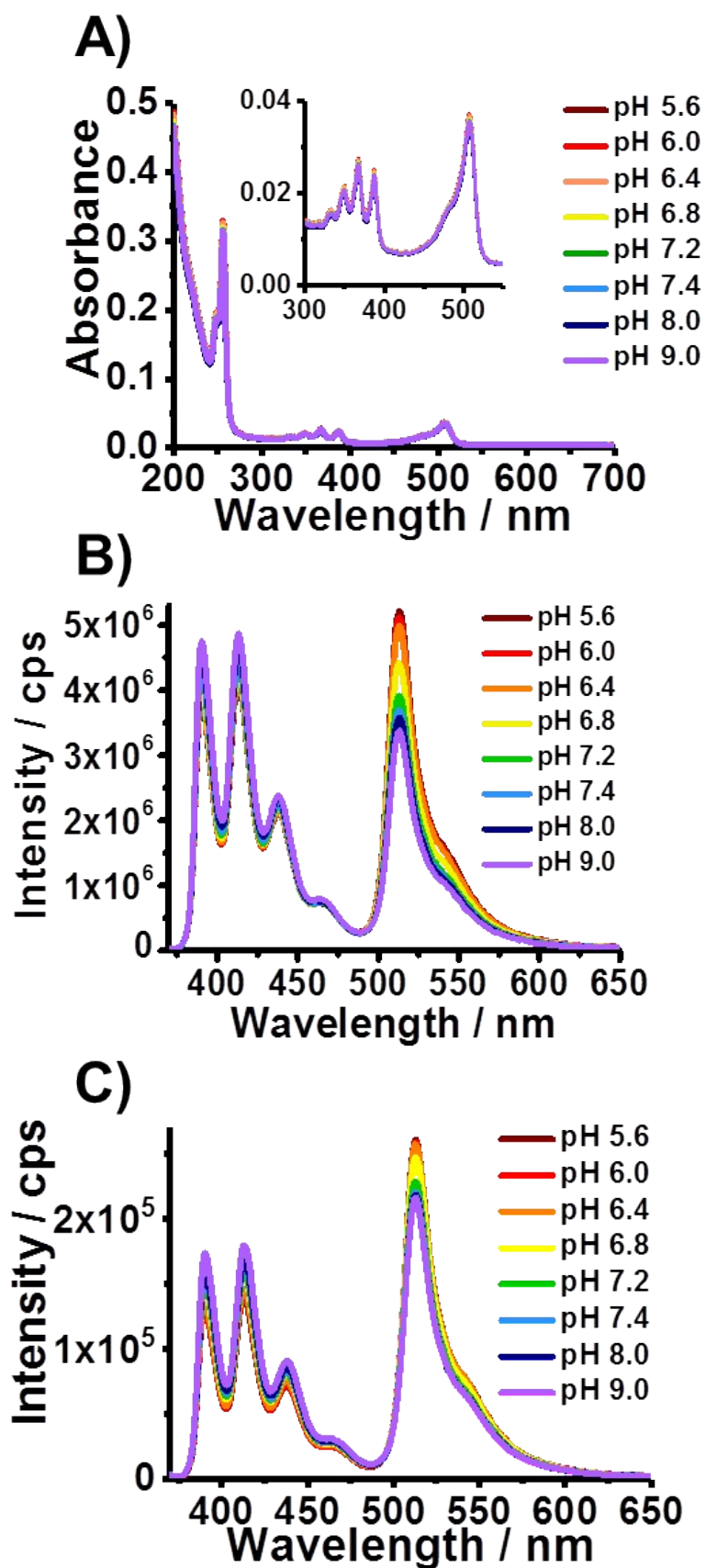
Figure S8. (A) UV-visible spectra, **(B)** PL spectra (λ_{ex} = 254 nm) and **(C)** PL spectra (λ_{ex} = 365 nm)

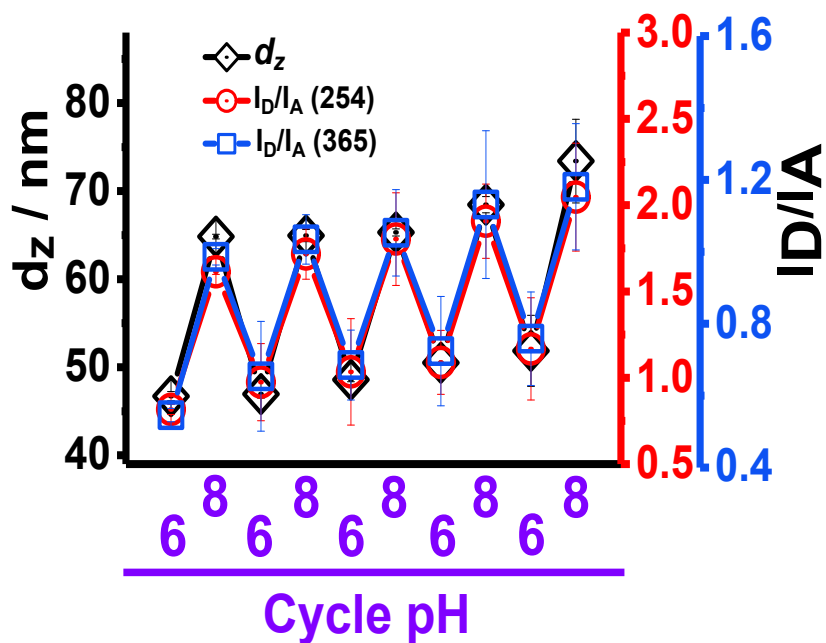for NG$_{AM/BDP}$ obtained at various pH values. The spectra in **(A)** are superimposed.

Figure S9. Reversibility of z-average diameter (d_z) and ratios of the donor and acceptor PL intensities (I_D/I_A) measured with excitation wavelengths of 254 and 365 nm for $NG_{AM/BDP}$ dispersions at pH values of 6 and 8.
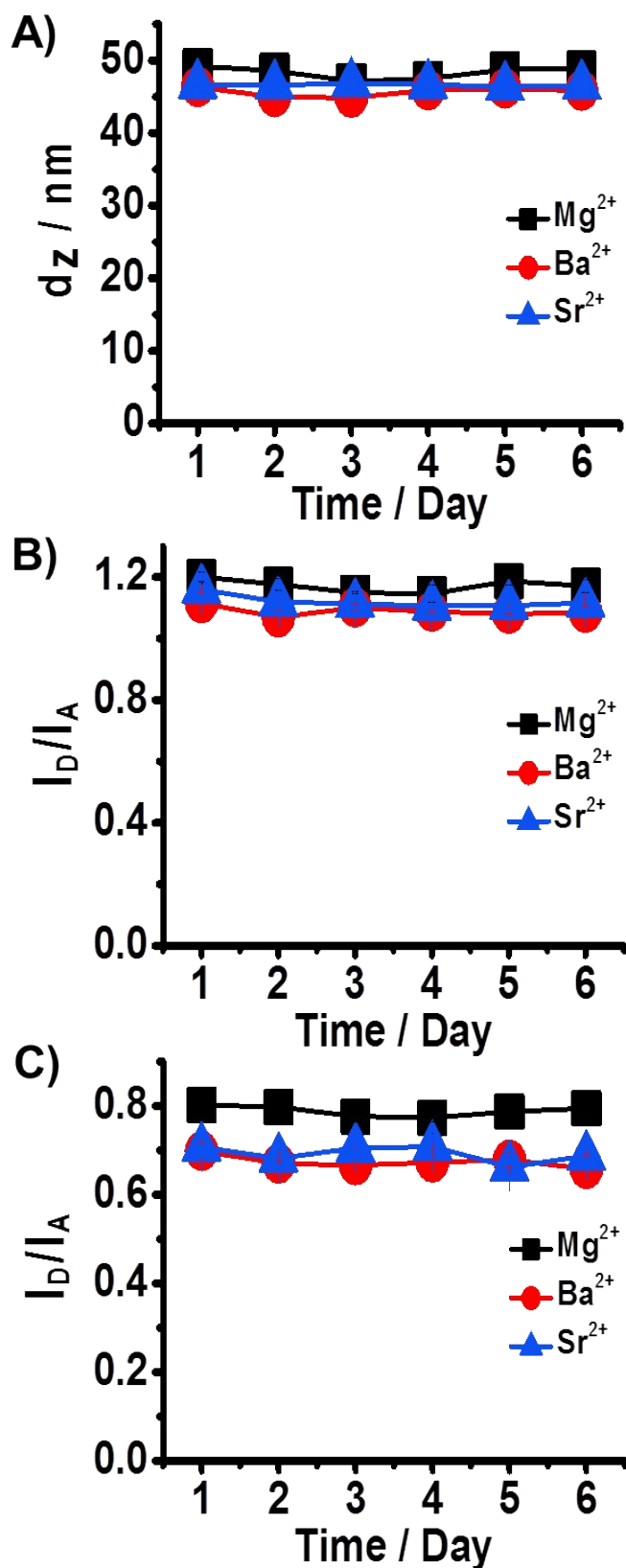
Figure S10. Variation of d_z **(A)** and I_D/I_A with excitation wavelengths of **(B)** 254 nm and **(C)** 365 nm for $NG_{AM/BDP}$ dispersions with time measured in the presence of aqueous Mg^{2+}, Ba^{2+} and Sr^{2+} solutions (30 mM) at pH 8.6.
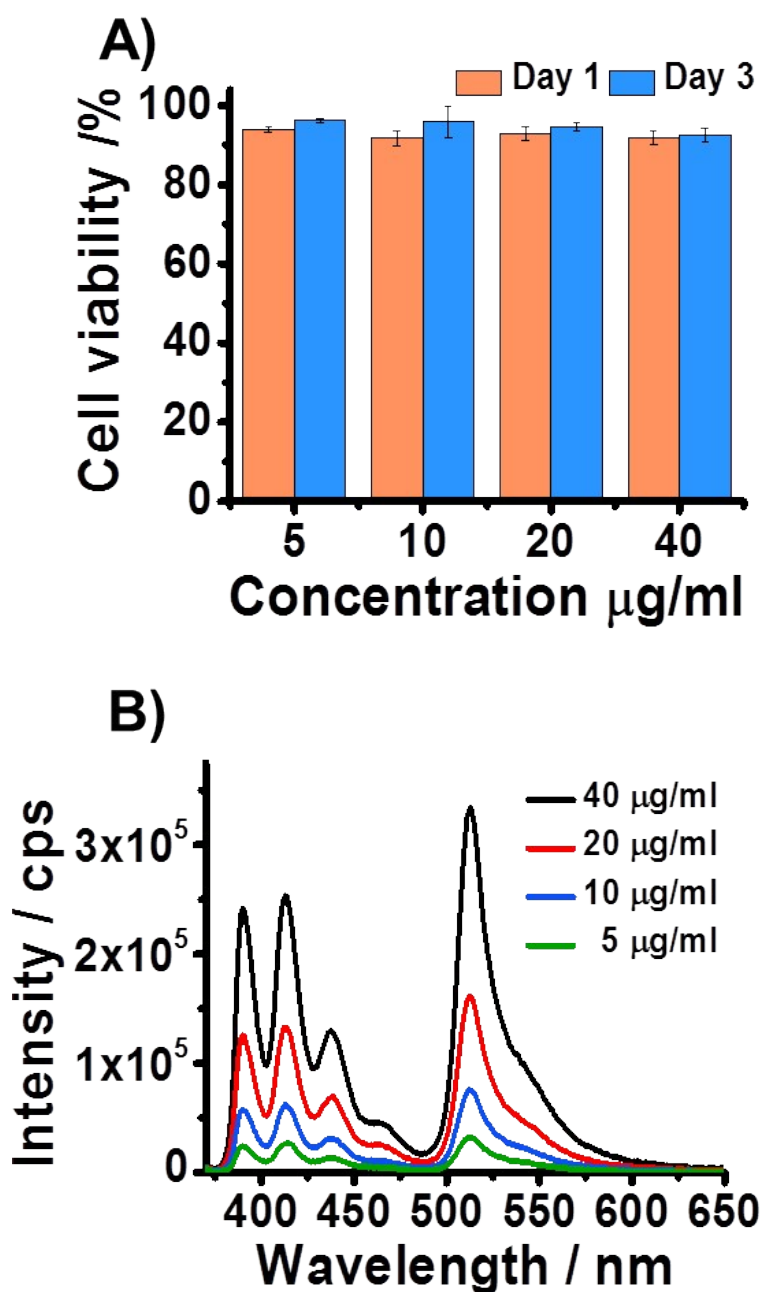
Figure S11. (A) Cell viability for human adipose-derived stem cells at various $NG_{AM/BDP}$ concentrations after 1 and 3 days. The data represent the mean value ± standard deviation (n = 3). **(B)** PL spectra (λ_{ex}= 365 nm) from the $NG_{AM/BDP}$ nanoprobes at various concentrations in PBS solution. These data show that $NG_{AM/BDP}$ does not have significant cytotoxicity at concentrations where PL can be readily detected.
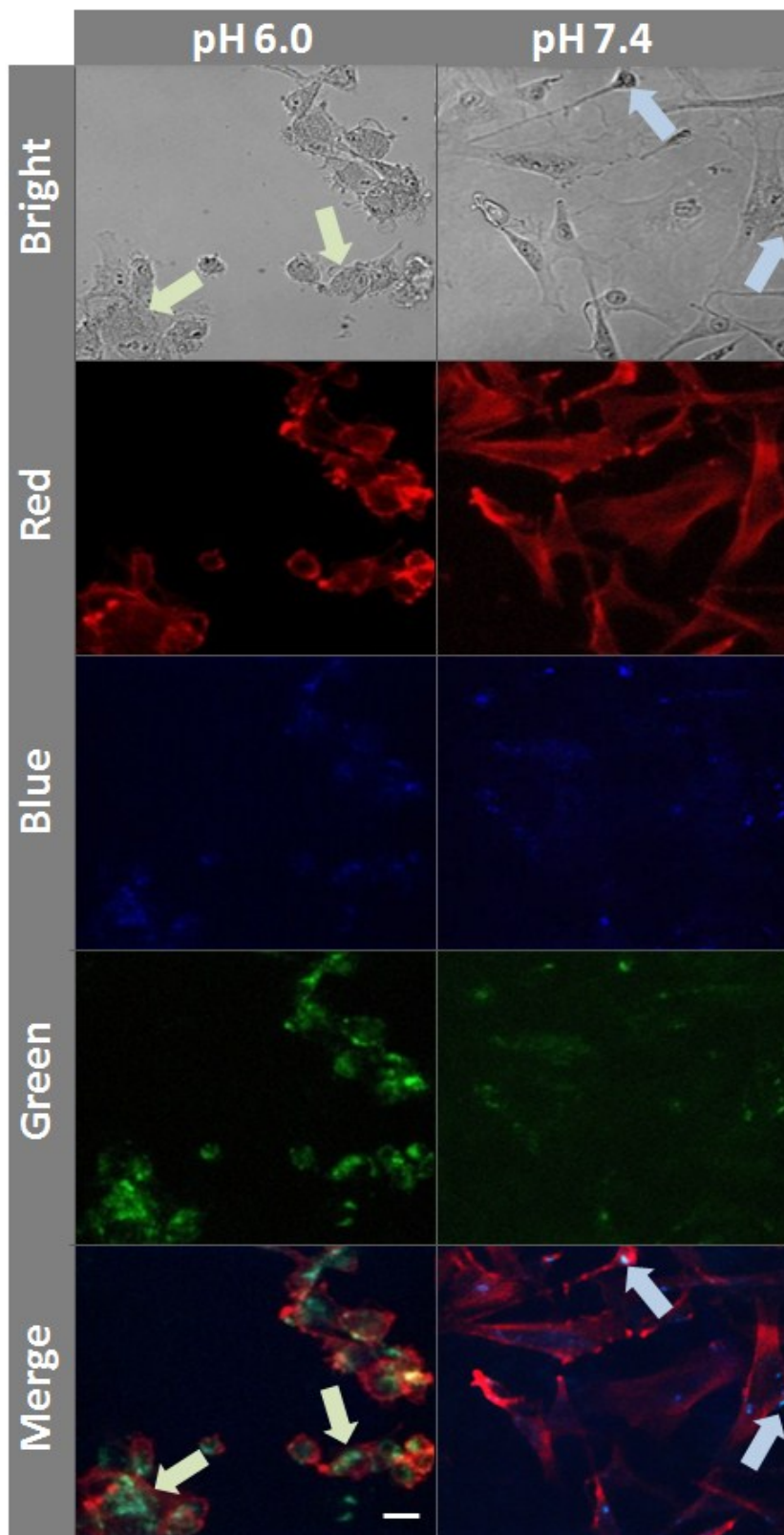
Figure S12. Cellular imaging and localization of NG$_{AM/BDP}$ particles (10 μg/mL) with a laser scanning confocal fluorescence microscope in stem cells using different (and merged) colour channels. The medium pH is shown. The arrows show the location of NG$_{AM/BDP}$ uptake in the cells. The top image is from white light. The scale bar is 25 μm and applies to all images.
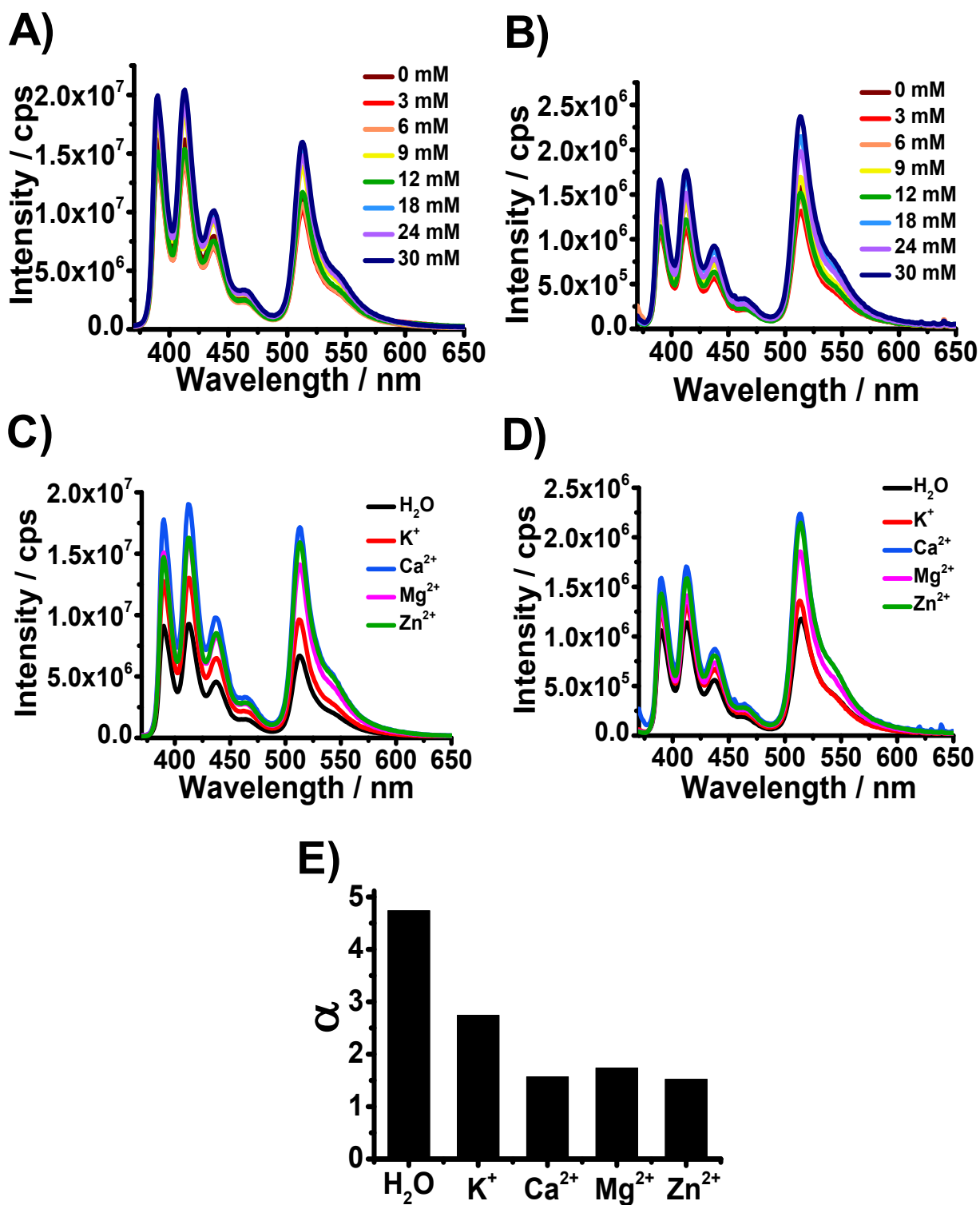
Figure S13. PL spectra for DX NG-*MAA*(NG$_{AM/BDP}$) measured at **(A)** 254 and **(B)** 365 nm at various concentrations of Mg^{2+}, **(C)** 254 nm and **(D)** 365 nm at different type of 30 mM ions (pH 7.4 buffer solution). **(E)** Variation of the linear swelling ratio, α, in the presence of the ions.
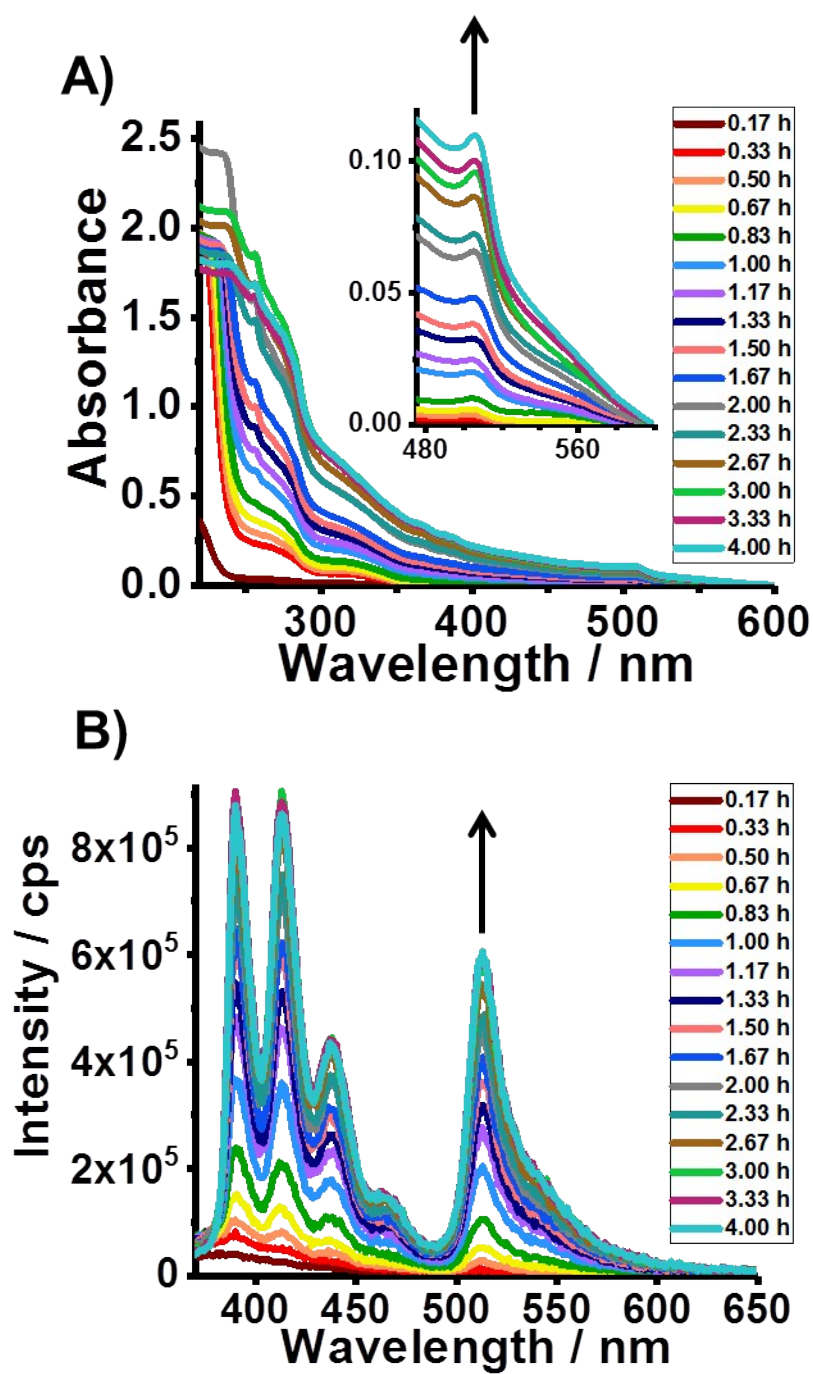
Figure S14. (A) UV-visible spectra and **(B)** PL spectra (λ_{ex} = 254 nm) of supernatant obtained during the degradation of Gelatin(NG$_{\text{AM/BDP}}$) gels at 32 °C over different times. The pH was 7.4.

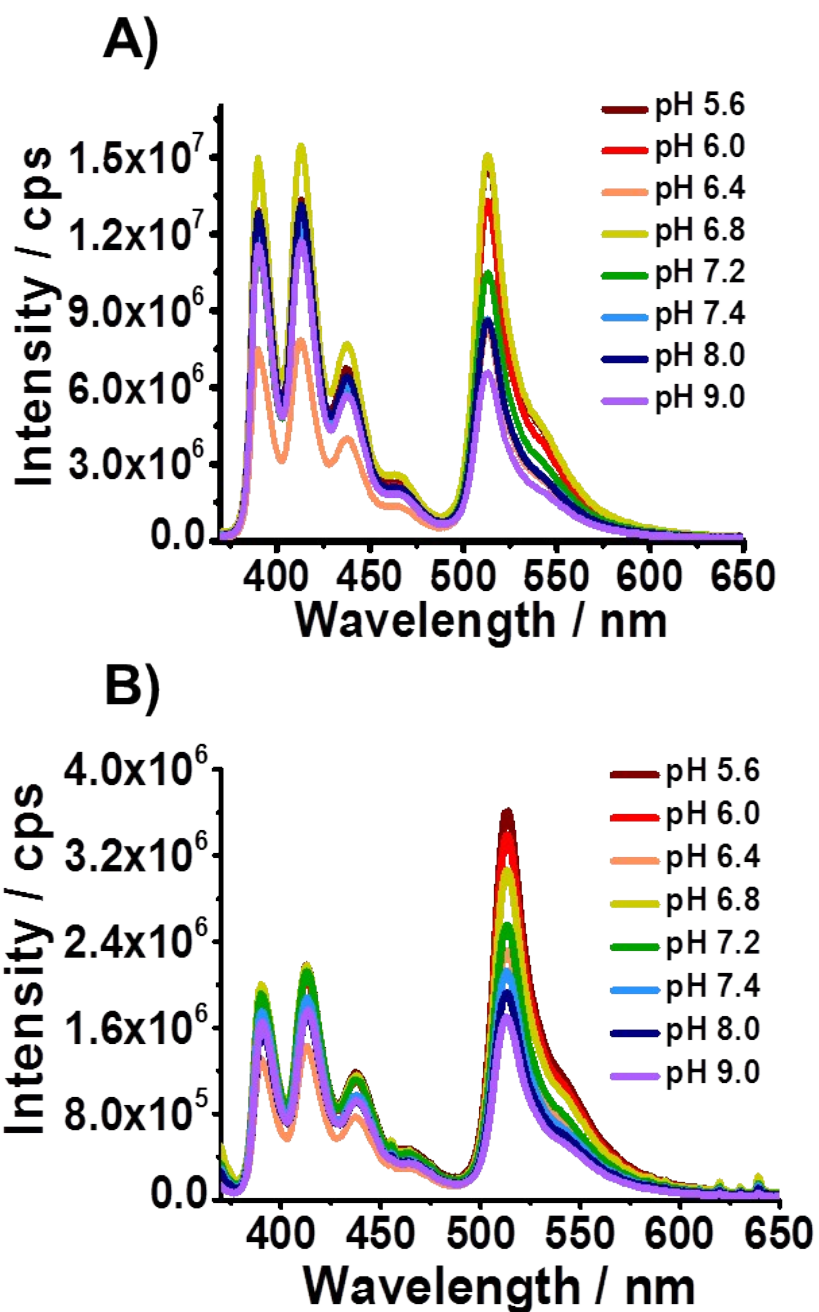**Figure S15.** PL spectra for Gelatin(NG$_{AM/BDP}$) in buffers with various pH values measured at 25 °C using **(A)** 254 nm and **(B)** 365 nm.
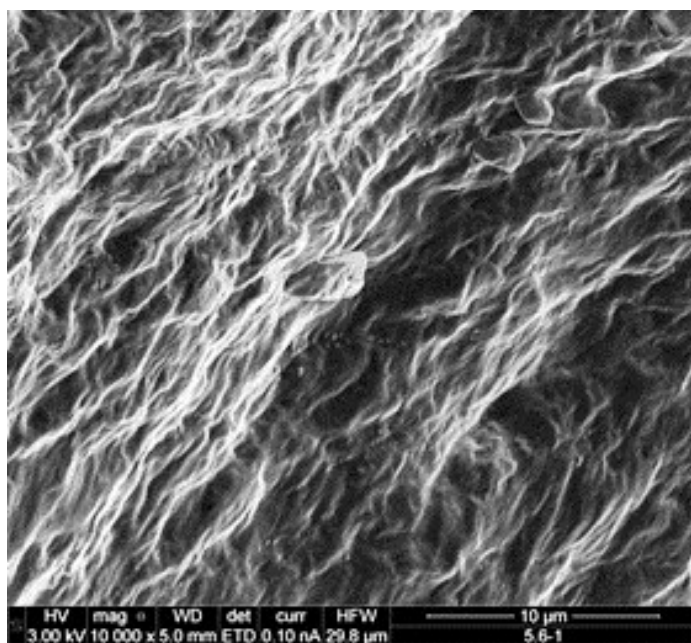
Figure S16. SEM image for Gelatin(NG$_{AM/BDP}$) gel freeze-dried at a pH 5.6. Scale bar: 10 μm.
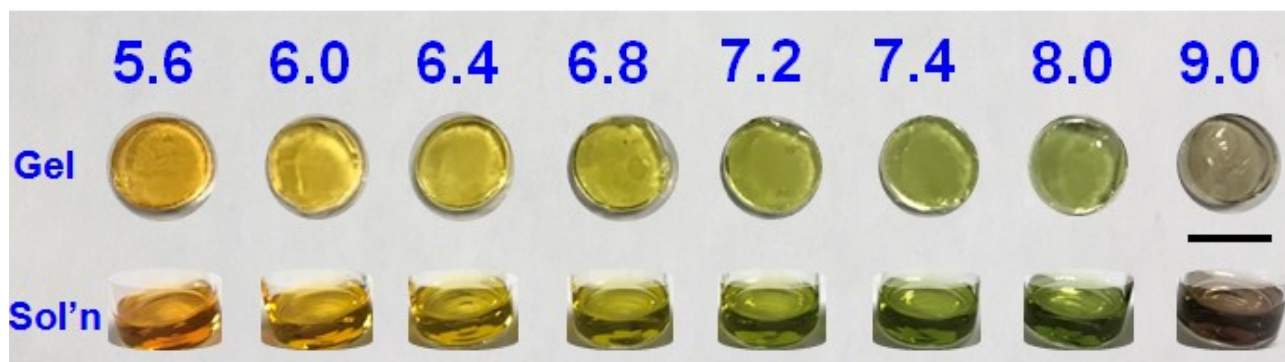
Figure S17. Digital photographs of Gelatin(NG$_{AM/BDP}$) gels (top) containing universal pH indicator. The pH values are shown. The solutions of indicator at the same respective pH values are shown immediately below each gel. The scale bar is 10 mm.
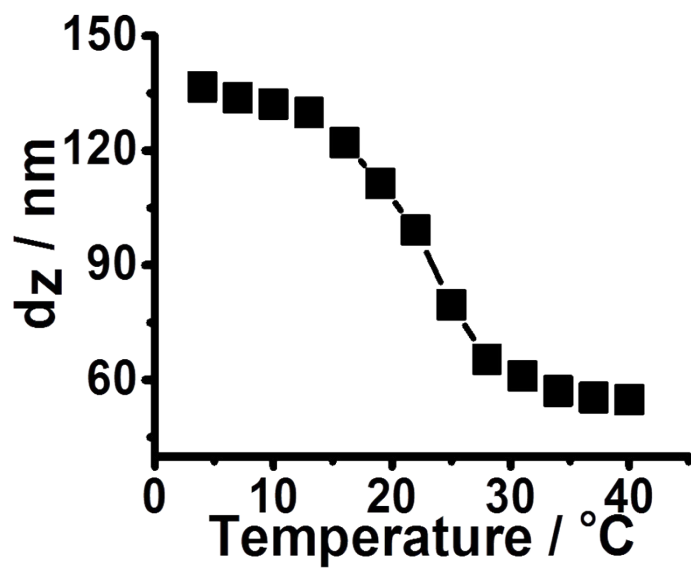
Figure S18. Variation of d_z with temperature for the NG-OEG_{GMA} based OEGMA particles.

Figure S19. PL spectra of DX NG-*OEG*(NG$_{AM/BDP}$) measured at various temperatures using 365 nm excitation at pH 6.0.
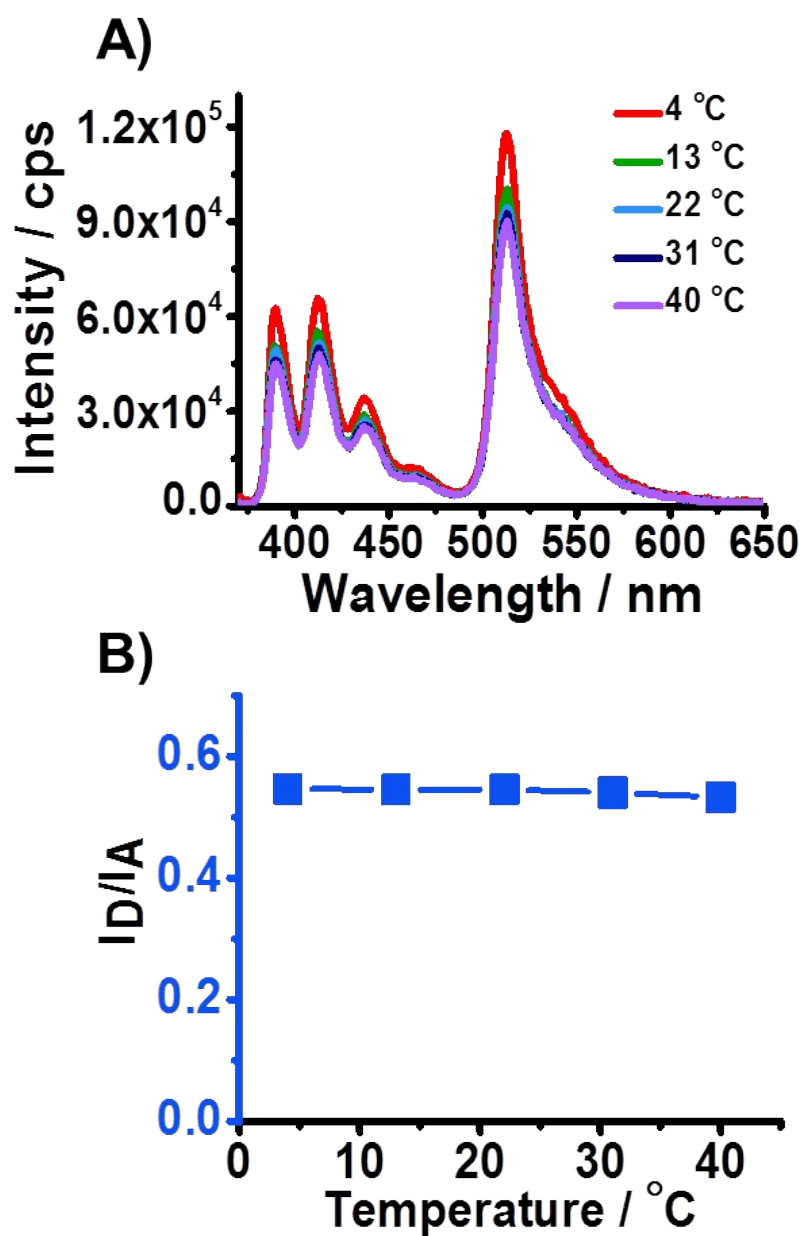
Figure S20. (A) PL spectra of $NG_{AM/BDP}$ at different temperature. **(B)** Plot of I_D/I_A vs temperature for $NG_{AM/BDP}$ ($\lambda_{ex} = 254$ nm).
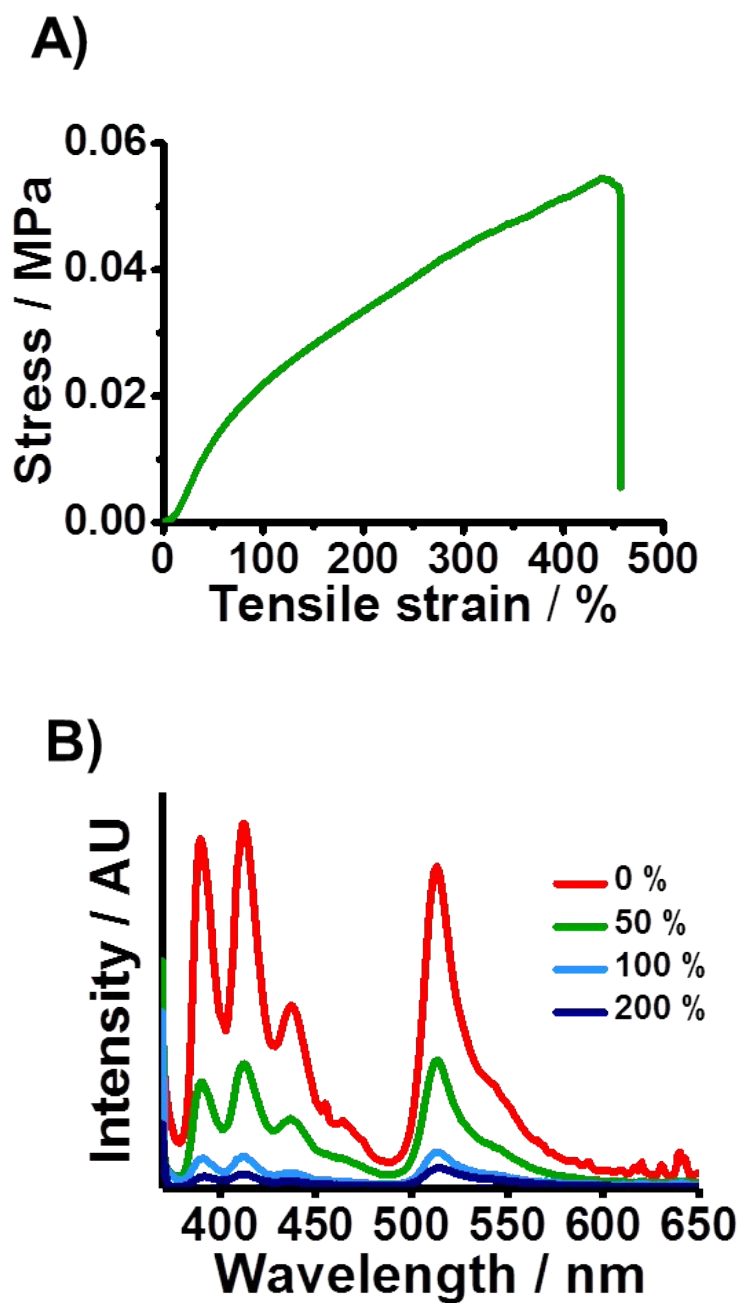
Figure S21. (A) Tensile stress-strain data for PAAm-Clay(NG$_{AM/BDP}$) gel. **(B)** PL spectra measured at 365 nm at selected tensile strains.

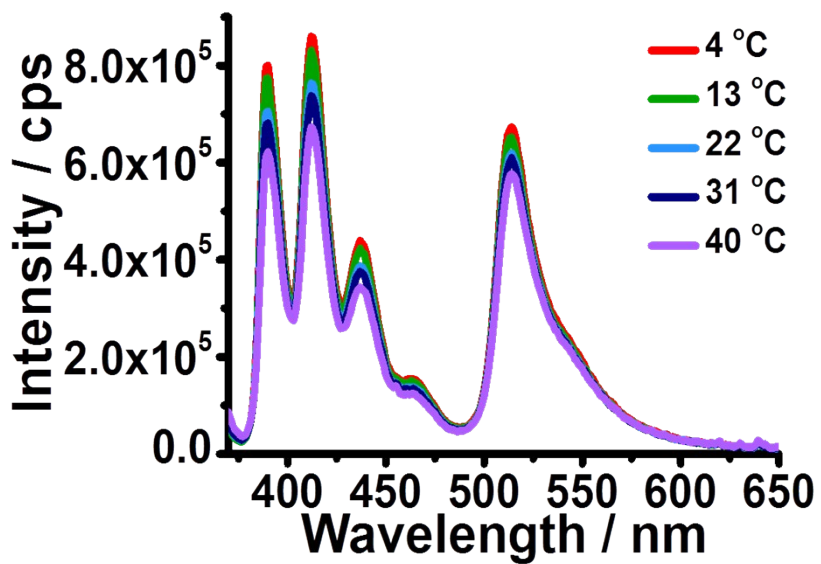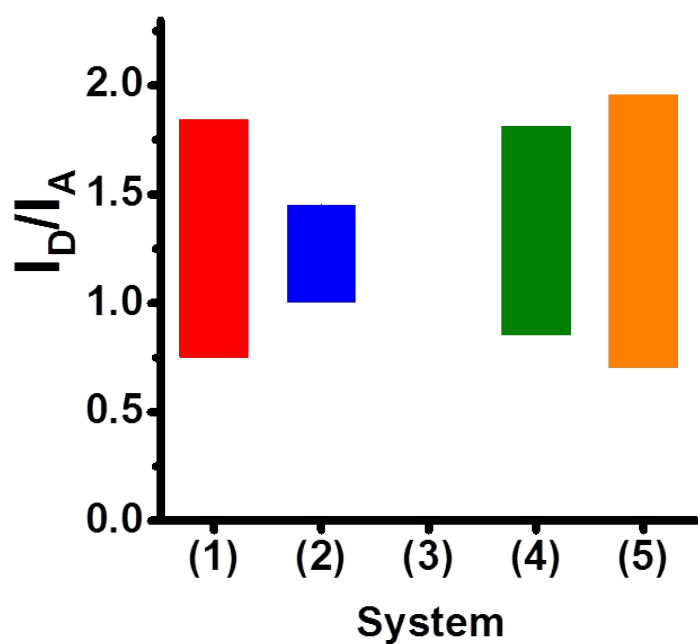| Number	System	Response
(1)	NG$_{AM/BDP}$	pH & ions
(2)	DX NG-*MAA*(NG$_{AM/BDP}$)	Ions
(3)	DX NG-OEG(NG$_{AM/BDP}$)	Temperature
(4)	Gelatin(NG$_{AM/BDP}$)	pH
(5)	PAAm-Clay(NG$_{AM/BDP}$)	Stretching

Figure S22. I_D/I_A ranges (λ_{ex} = 254 nm) for NGs reported in this study. System (3) scattered light strongly at low wavelengths which meant that the I_D/I_A values were not reliable using λ_{ex} = 254 nm.
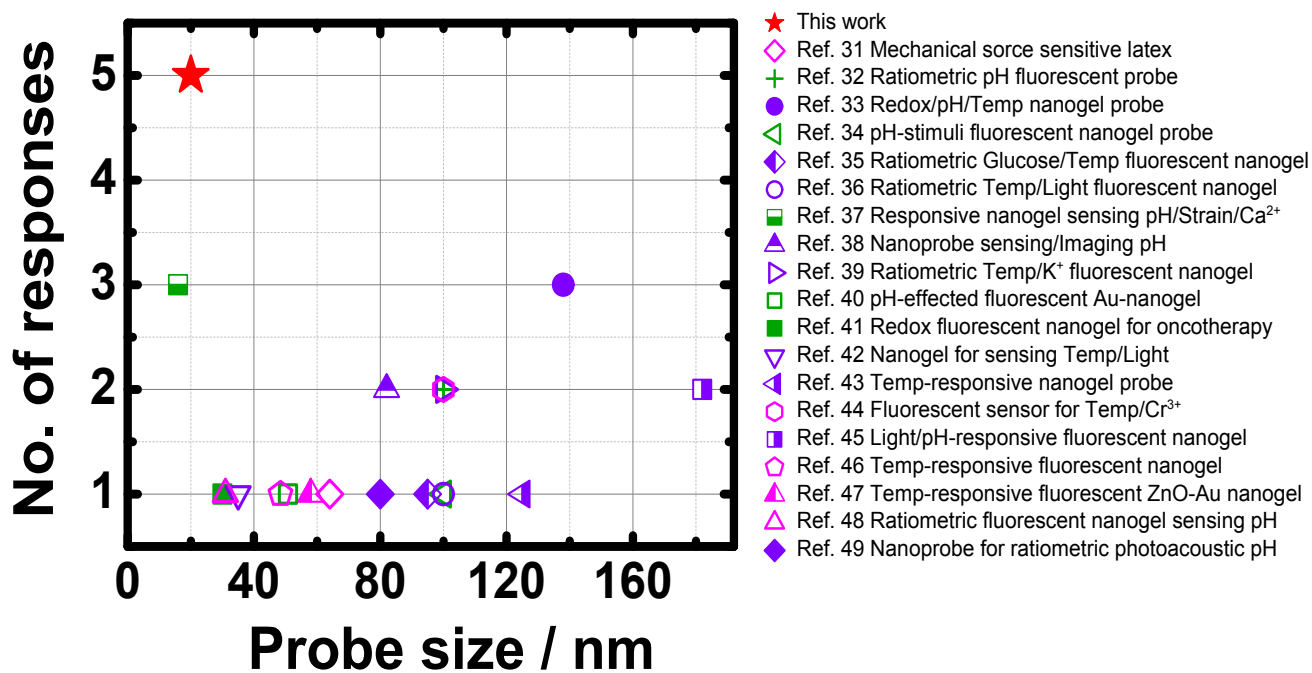
Figure S23. Comparison of number of responses reported for various nanogel probes. The data used is shown in Table S3.

TABLES

Table S1. Materials Used to Prepare the Nanogel Particles.

Nanogel	MMA / wt.%[a]	MEO$_2$MA / wt.%[a]	OEGMA/ wt.%[a]	MAA / wt.%[a]	EGD / wt.%[a]	SDS / wt.%[b]	AM / wt.%[a]	APS/ wt.%[b]	Total / g[c]	Water / g
NG$_{AM/BDP}$	78.8	-	-	18.8	2.01	0.51	0.38	0.05	53.3	240
NG$_{AM}$	78.8	-	-	18.8	2.01	0.51	0.38	0.05	53.3	240
NG$_{BDP}$	79.1	-	-	18.8	2.00	0.51	-	0.07	53.1	240
NG-MAA_{GMA}[d]	79.1	-	-	18.8	2.00	0.51	-	0.07	53.1	240
NG-OEG_{GMA}[e]	-	80.3	8.9	10.6	0.20	0.02	-	0.02	2.77	252

[a] With respect to monomer. [b] Dissolved in water phase. [c] Total mass of all monomers added. [d] Nanogel matrixes used to prepare the DX NG-MAA(NG$_{AM/BDP}$) gels. [e] Nanogel matrixes used to prepare the DX NG-OEG(NG$_{AM/BDP}$) gels.

Table S2. Composition and Properties of the Nanogel Particles.

Nanogel	MAA^a/ mol%	GMA/ mol%	AM ^{b}/ mol%	BDP ^{b} / mol%	μ/ x 10^{-8} m^2 / Vs^c	pK_a^{d}	d_{TEM} /nm (CV) ^{e}	$d_{5.6}$^{f} / nm	$d_{9.0}$^{f} / nm
NG$_{AM/BDP}$	34.76	-	0.24	0.11	-1.02	7.1	20 (4)	46	65
NG$_{AM}$	34.79	-	0.24	-	-1.11	7.0	21 (5)	47	76
NG$_{BDP}$	36.87	-	-	0.09	-1.17	7.0	19 (5)	42	64
NG-MAA_{GMA}	30.95	5.94	-	-	-1.06	6.9	18 (4)	34	83
NG-OEG_{GMA}	20.27	4.41	-	-	-	5.9	58 (7)	-	-

^{a} Calculated from potentiometric titration data shown in Figure S1. ^{b} Determined from UV-visible spectroscopy data using the Beer-Lambert law (Figure S1). ^{c} Electrophoretic mobility at pH 5.6. ^{d} Apparent pK_a values were obtained from data (Figure S4). ^{e} Number-average diameters determined from TEM images (Fig. S3A to S3C, ESI†). The number in brackets is the coefficient of variation. ^{f} z-average diameter at pH values of 5.6 and 9.0.

Table S3. A List and primary review of recent years on performance comparison of photoluminescence nanoprobe. (☑ : yes, ✗ : No, ~ : Estimate)

System	Synthetic Process	D-d_z / nm[a]	H-d_z / nm[b]	pH	Temp	Ions	Mechanics	Degradation	Ref.	Year
Crystals	Seed-mediated	~27	31	✗	✗	☑	✗	✗	6	2015
Crystals	Precipitation	16	✗	✗	✗	☑	✗	✗	7	2015
Crystals	Coupling	✗	24	☑	✗	✗	✗	✗	8	2018
Crystals	Solvothermal	24.7	✗	✗	✗	☑	✗	✗	9	2018
Crystals	Precipitation	100	6	☑	✗	✗	✗	✗	10	2016
Hybrids	Precipitation	50	151.6	☑	☑	✗	✗	☑	11	2016
Hybrids	ATRP[c]	~50	~110	☑	☑	✗	✗	✗	12	2012
Hybrids	Self-assembly	60	70	☑	✗	✗	✗	✗	13	2014
Hybrids	Assembly	~33	68.3	☑	✗	✗	✗	✗	14	2014
Hybrids	Silicification	31.5	48.9	✗	✗	✗	✗	☑	15	2012
Hybrids	Coupling	50	98.2	✗	✗	☑	✗	✗	16	2017
Hybrids	Condensation	~120	295	✗	✗	✗	✗	☑	17	2015
Hybrids	Assembly	✗	25.1	☑	✗	✗	✗	✗	4	2012
Hybrids	RAFT[d]	~10	30	☑	✗	✗	✗	✗	18	2014
Hybrids	Precipitation	~6	8.5	☑	✗	✗	✗	✗	19	2016
Hybrids	ATRP	~28	8.7	☑	✗	✗	✗	✗	20	2017
Hybrids	Precipitation	140	~200	☑	✗	✗	✗	✗	21	2016
Hybrids	Precipitation	27	~40	✗	✗	✗	✗	✗	22	2012
Hybrids	Sedimentation	87	145	✗	✗	☑	✗	✗	23	2018
Micelles	Self-assembly	50	61.6	☑	✗	✗	✗	✗	24	2012
Micelles	Self-assembly	~21	33.8	✗	✗	☑	✗	☑	25	2017
Micelles	RAFT	✗	49	☑	☑	✗	✗	✗	26	2010
Micelles	Precipitation	~24	22.7	☑	✗	✗	✗	✗	27	2017

Micelles	ATRP	✗	7.3	☑	✗	✗	✗	✗	28	2014
Micelles	ATRP	~38	3	☑	✗	✗	✗	✗	29	2012
Micelles	Precipitation	~122	138.4	☑	✗	✗	✗	✗	30	2015
Nanogels	Poly-emulsion	✗	64	✗	✗	✗	☑	✗	31	2017
Nanogels	Assembly	~100	92	☑	✗	☑	✗	✗	32	2014
Nanogels	Poly-emulsion	138	102	☑	☑	✗	✗	☑	33	2015
Nanogels	Assembly	~100	14.8	☑	✗	✗	✗	✗	34	2012
Nanogels	Poly-emulsion	95	43	✗	☑	✗	✗	✗	35	2011
Nanogels	Poly-emulsion	100	30	✗	☑	✗	✗	✗	36	2011
Nanogels	Poly-emulsion	16	24	☑	✗	☑	☑	✗	37	2017
Nanogels	Precipitation	✗	~82	☑	☑	✗	✗	✗	38	2010
Nanogels	Poly-emulsion	100	46	✗	☑	☑	✗	✗	39	2010
Nanogels	Assembly	50.8	202	☑	✗	✗	✗	✗	40	2016
Nanogels	Precipitation	30	40	☑	✗	✗	✗	✗	41	2017
Nanogels	Poly-emulsion	35	75	✗	☑	✗	✗	✗	42	2017
Nanogels	Poly-emulsion	~125	~65	✗	☑	✗	✗	✗	43	2015
Nanogels	Poly-emulsion	20	45.6	☑	☑	☑	☑	☑	This work	2019
Nanogels	Poly-emulsion	100	50	✗	☑	☑	✗	✗	44	2014
Nanogels	Poly-emulsion	182	~100	☑	☑	✗	✗	✗	45	2015
Nanogels	Poly-emulsion	48.4	✗	✗	☑	✗	✗	✗	46	2018
Nanogels	Poly-solution	58	~13	✗	☑	✗	✗	✗	47	2011
Nanogels	Precipitation	~31	125	☑	✗	✗	✗	✗	48	2010
Nanogels	Self-assembly	80	125	☑	✗	✗	✗	✗	49	2015

[a] Dried size calculated from electron microscope, [b] Hydraulic size calculated from dynamic light scattering, [c] Atom transfer radical polymerization, [d] Reversible Addition Fragmentation Chain Transfer.

REFERENCES

1   Y. X. Zhu, Z. W. Wei, M. Pan, H. P. Wang, J. Y. Zhang and C. Y. Su, *Dalton Trans.*, 2016, **45**, 943-950.
2   E. A. Grulke, E. Immergut and J. Brandrup, *Polymer handbook*, John Wiley & Sons, 1999.
3   J. R. Lakowicz, *Principles of fluorescence spectroscopy*, Springer, New York, 2006.
4   A. M. Dennis, W. J. Rhee, D. Sotto, S. N. Dublin and G. Bao, *ACS Nano*, 2012, **6**, 2917-2924.
5   C. Ma, F. Zeng, L. F. Huang and S. Z. Wu, *J. Phys. Chem. B*, 2011, **115**, 874-882.
6   Z. Li, S. W. Lv, Y. L. Wang, S. Y. Chen and Z. H. Liu, *J. Am. Chem. Soc.*, 2015, **137**, 3421-3427.
7   J. J. Peng, W. Xu, C. L. Teoh, S. Y. Han, B. Kim, A. Samanta, J. C. Er, L. Wang, L. Yuan, X. G. Liu and Y. T. Chang, *J. Am. Chem. Soc.*, 2015, **137**, 2336-2342.
8   T. C. Ma, Y. Hou, J. F. Zeng, C. Y. Liu, P. S. Zhang, L. H. Jing, D. Shangguan and M. Y. Gao, *J. Am. Chem. Soc.*, 2018, **140**, 211-218.
9   Y. Liu, A. Jiang, Q. Jia, X. Zhai, L. Liu, L. Ma and J. Zhou, *Chem. Sci.*, 2018.
10 H. P. Xia, F. Y. Li, W. Park, S. F. Wang, Y. Jang, Y. Du, S. Baik, S. Cho, T. Kang, D. H. Kim, D. S. Ling, K. M. Hui and T. Hyeon, *ACS Cent. Sci.*, 2016, **2**, 802-811.
11 Y. Liu, Z. T. Wang, H. M. Zhang, L. X. Lang, Y. Ma, Q. J. He, N. Lu, P. Huang, Y. J. Liu, J. B. Song, Z. B. Liu, S. Gao, Q. J. Ma, D. O. Kiesewetter and X. Y. Chen, *Nanoscale*, 2016, **8**, 10553-10557.
12 M. S. Strozyk, M. Chanana, I. Pastoriza-Santos, J. Perez-Juste and L. M. Liz-Marzan, *Adv. Funct. Mater.*, 2012, **22**, 1436-1444.
13 D. Ling, W. Park, S. J. Park, Y. Lu, K. S. Kim, M. J. Hackett, B. H. Kim, H. Yim, Y. S. Jeon, K. Na and T. Hyeon, *J. Am. Chem. Soc.*, 2014, **136**, 5647-5655.
14 Y. Y. Yuan, D. Ding, K. Li, J. Liu and B. Liu, *Small*, 2014, **10**, 1967-1975.
15 E. Mahon, D. R. Hristov and K. A. Dawson, *Chem. Commun.*, 2012, **48**, 7970-7972.
16 Y. Liu, S. Wang, Y. Ma, J. Lin, H. Y. Wang, Y. Gu, X. Chen and P. Huang, *Adv. Mater.*, 2017, **29**, 1606129.
17 Y. Fatieiev, J. G. Croissant, K. Julfakyan, L. Deng, D. H. Anjum, A. Gurinov and N. M. Khashab, *Nanoscale*, 2015, **7**, 15046-15050.
18 K. Paek, H. Yang, J. Lee, J. Park and B. J. Kim, *ACS Nano*, 2014, **8**, 2848-2856.
19 Q. Q. Miao, Y. Lyu, D. Ding and K. Y. Pu, *Adv. Mater.*, 2016, **28**, 3662-3668.
20 Y. Wang, C. Wang, Y. Li, G. Huang, T. Zhao, X. Ma, Z. Wang, B. D. Sumer, M. A. White and J. Gao, *Adv. Mater.*, 2017, **29**, 1603794.
21 L. G. Yang, C. F. Cui, L. Z. Wang, J. Y. Lei and J. L. Zhang, *ACS Appl. Mater. Interfaces*, 2016, **8**, 19084-19091.
22 L. Q. Xiong, A. J. Shuhendler and J. H. Rao, *Nat. Commun.*, 2012, **3**.
23 P. Wang, F. Zhou, C. Zhang, S.-Y. Yin, L. Teng, L. Chen, X. Hu, H. Liu, X. Yin and X. Zhang, *Chem. Sci.*, 2018.
24 W. Wang, D. Cheng, F. Gong, X. Miao and X. Shuai, *Adv. Mater.*, 2012, **24**, 115-120.
25 C. Yin, X. Zhen, Q. L. Fan, W. Huang and K. Y. Pu, *ACS Nano*, 2017, **11**, 4174-4182.
26 C. H. Li, Y. X. Zhang, J. M. Hu, J. J. Cheng and S. Y. Liu, *Angew. Chem., Int. Ed.*, 2010, **49**, 5120-5124.
27 L. Chen, L. Wu, J. Yu, C.-T. Kuo, T. Jian, I.-C. Wu, Y. Rong and D. Chiu, *Chem. Sci.*, 2017, **8**, 7236-7245.
28 X. P. Ma, Y. G. Wang, T. Zhao, Y. Li, L. C. Su, Z. H. Wang, G. Huang, B. D. Sumer and J. M. Gao, *J. Am. Chem. Soc.*, 2014, **136**, 11085-11092.
29 K. J. Zhou, H. M. Liu, S. R. Zhang, X. N. Huang, Y. G. Wang, G. Huang, B. D. Sumer and J. M. Gao, *J. Am. Chem. Soc.*, 2012, **134**, 7803-7811.
30 J. W. Tian, J. F. Zhou, Z. Shen, L. Ding, J. S. Yu and H. X. Ju, *Chem. Sci.*, 2015, **6**, 5969-5977.
31 M. Li, W. F. Liu, Q. Zhang and S. P. Zhu, *ACS Appl. Mater. Interfaces*, 2017, **9**, 15156-15163.

32 L. X. Cao, X. Y. Li, S. Q. Wang, S. Y. Li, Y. Li and G. Q. Yang, *Chem. Commun.*, 2014, **50**, 8787-8790.

33 S. F. Lou, S. Gao, W. W. Wang, M. M. Zhang, J. Zhang, C. Wang, C. Li, D. L. Kong and Q. Zhao, *Nanoscale*, 2015, **7**, 3137-3146.

34 H. S. Park, J. E. Lee, M. Y. Cho, J. H. Hong, S. H. Cho and Y. T. Lim, *Macromol. Rapid Commun.*, 2012, **33**, 1549-1555.

35 D. Wang, T. Liu, J. Yin and S. Y. Liu, *Macromolecules*, 2011, **44**, 2282-2290.

36 J. Yin, H. B. Hu, Y. H. Wu and S. Y. Liu, *Polym. Chem.*, 2011, **2**, 363-371.

37 M. N. Zhu, D. D. Lu, S. L. Wu, Q. Lian, W. K. Wang, A. H. Milani, Z. X. Cui, N. T. Nguyen, M. Chen, L. A. Lyon, D. J. Adlam, A. J. Freemont, J. A. Hoyland and B. R. Saunders, *ACS Macro Lett.*, 2017, **6**, 1245-1250.

38 Y. L. Chiu, S. A. Chen, J. H. Chen, K. J. Chen, H. L. Chen and H. W. Sung, *ACS Nano*, 2010, **4**, 7467-7474.

39 J. Yin, C. H. Li, D. Wang and S. Y. Liu, *J. Phys. Chem. B*, 2010, **114**, 12213-12220.

40 N. Goswami, F. X. Lin, Y. B. Liu, D. T. Leong and J. P. Xie, *Chem. Mater.*, 2016, **28**, 4009-4016.

41 J. J. Chen, J. X. Ding, W. G. Xu, T. M. Sun, H. H. Xiao, X. L. Zhuang and X. S. Chen, *Nano Lett.*, 2017, **17**, 5180-5180.

42 S. H. Lee, H. T. Bui, T. P. Vales, S. Cho and H. J. Kim, *Dyes Pigm.*, 2017, **145**, 216-221.

43 J. Liu, X. D. Guo, R. Hu, J. Xu, S. Q. Wang, S. Y. Li, Y. Li and G. Q. Yang, *Anal. Chem.*, 2015, **87**, 3694-3698.

44 X. J. Wan, H. Y. Liu, S. Yao, T. Q. Liu and Y. W. Yao, *Macromol. Rapid Commun.*, 2014, **35**, 323-329.

45 H. Wang, J. Di, Y. B. Sun, J. P. Fu, Z. Y. Wei, H. Matsui, A. D. Alonso and S. Q. Zhou, *Adv. Funct. Mater.*, 2015, **25**, 5537-5547.

46 S. Uchiyama, T. Tsuji, K. Kawamoto, K. Okano, E. Fukatsu, T. Noro, K. Ikado, S. Yamada, Y. Shibata, T. Hayashi, N. Inada, M. Kato, H. Koizumi and H. Tokuyama, *Angew. Chem., Int. Ed.*, 2018, **57**, 5413-5417.

47 W. T. Wu, J. Shen, P. Banerjee and S. Q. Zhou, *Adv. Funct. Mater.*, 2011, **21**, 2830-2839.

48 H. S. Peng, J. A. Stolwijk, L. N. Sun, J. Wegener and O. S. Wolfbeis, *Angew. Chem., Int. Ed.*, 2010, **49**, 4246-4249.

49 Q. Chen, X. Liu, J. Chen, J. Zeng, Z. Cheng and Z. Liu, *Adv. Mater.*, 2015, **27**, 6820-6827.